

A Treatise on the Numerical Simulation of the Compressible Fluid Flow in the Sealing Gap of the Screw Machines

Dipl.-Ing. J. Vimmr, Pilsen/CZ

Abstract

This paper is devoted to the numerical computation of the steady state compressible inviscid fluid flow through the two-dimensional model of the sealing gap between the stator and the head of the female rotor tooth in the screw compressor. The results obtained by means of the cell-centred finite volume formulation of the explicit Causon's simplified TVD MacCormack scheme on a structured quadrilateral grid are compared with the results gained by using the software package Fluent 5.3. The influence of the sealing gap geometry and of the choice of boundary conditions on the numerical results is shown in this paper. The comparison of the results obtained by the described numerical simulation with the experiment performed at the Technical University of Dortmund is discussed.

Zusammenfassung

Im vorliegenden Beitrag wird die numerische Simulation der stationären reibungsfreien Gasströmung in einem ebenen Modell des Nebenrotor-Gehäusespaltes im Schraubenkompressor dargestellt. Die Berechnung der Gasströmung wurde mit Hilfe der Methode der finiten Volumenelemente auf einem viereckigen Gitter durch das explizite Causons TVD MacCormack Schema und mit Hilfe der CFD-Software Fluent 5.3 durchgeführt. Diese Ergebnisse werden verglichen. Der Einfluss der Geometrie des Nebenrotor-Gehäusespaltes und der Randbedingungenformulierung auf die numerische Ergebnisse wird in diesem Beitrag gezeigt. Weiter wird eine Vergleichung der numerisch berechneten Ergebnissen mit experimentellen Ergebnissen, die auf TU Dortmund gewonnen wurden, diskutiert.

1 Introduction

The mathematical modelling of compressible flows belongs to challenging problems of internal aerodynamics, examples of which can be found in many areas of industry, for instance in screw compressors and turbines operation. The processes which take place in the work space and in the gaps on its boundary have a great influence on the performance of the screw compressor, especially with regard to its internal efficiency. The most important gaps in the screw compressor are the sealing gaps which have also a great influence on the internal efficiency of the

screw compressor and can be probably the sources of noise. Therefore it is necessary to analyse the fluid flow through the sealing gap in the screw compressor. In this paper a numerical computation of the steady state compressible inviscid fluid flow through the two-dimensional model of the sealing gap in the screw compressor is shown.

2 Numerical simulation of fluid flow through the sealing gap

2.1 Formulation of the problem

Let us consider the sealing gap between the stator and the head of the female rotor tooth, Fig. 1 and Fig. 2, and accept the following restrictions. We will assume that the female rotor does not move and that the sealing gap can be simulated by a two-dimensional bounded domain $\Omega \subset \mathbb{R}^2$ occupied by the compressible inviscid fluid with the boundary $\partial\Omega = \partial\Omega_I \cup \partial\Omega_O \cup \partial\Omega_W$, where $\partial\Omega_I$ is the inlet and $\partial\Omega_O$ the outlet section of the computational domain Ω . $\partial\Omega_W$ are fixed impermeable walls of the domain corresponding to the stator and the head of the female rotor tooth. The steady state solution of the compressible inviscid fluid flow through the sealing gap in the screw compressor is chosen.

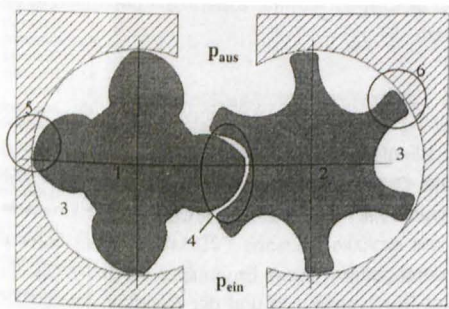


Fig. 1: Frontal section of rotors, 6 – female rotor-housing gap

Bild 1: Stirnschnitt der Rotoren, 6 – Nebenrotor-Gehäusespalt

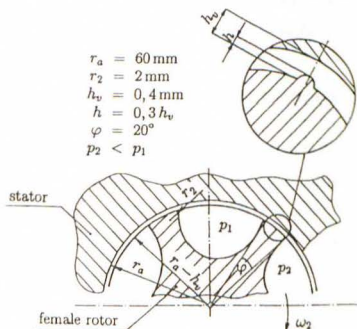


Fig. 2: Detail of female rotor-housing gap

Bild 2: Detail des Nebenrotor-Gehäusespaltes

2.2 Mathematical model of compressible inviscid fluid flow

The mathematical model of the two-dimensional compressible inviscid, non-heat-conducting fluid flow is described by the conservative system of the Euler equations, expressed in Eulerian description. In Cartesian coordinates the conservative system of the Euler equations can be written as

$$\frac{\partial w}{\partial t} + \frac{\partial f(w)}{\partial x} + \frac{\partial g(w)}{\partial y} = 0. \tag{1}$$

The vector of conservative variables w and Cartesian flux components $f(w)$ and $g(w)$ of the inviscid flux $\mathcal{H}(w) = (f(w), g(w))$ are defined as

$$\begin{aligned} w &= (\varrho, \varrho u, \varrho v, e)^T, \\ f(w) &= (\varrho u, \varrho u^2 + p, \varrho uv, (e + p)u)^T, \\ g(w) &= (\varrho v, \varrho uv, \varrho v^2 + p, (e + p)v)^T, \end{aligned} \quad (2)$$

where t is time, ϱ is density, p static pressure, e total energy per unit volume and $v = (u, v)^T$ is the velocity vector. The external volume forces are neglected.

The conservative system of the Euler equations (1) – (2) has to be completed with an equation of state $p = p(\varrho, T)$ defining the thermodynamical properties of the considered fluid. In the case of a perfect gas the equation of state can be written as

$$p = \varrho r T, \quad (3)$$

where $r = 287 \text{ J kg}^{-1} \text{ K}^{-1}$ is the gas constant per unit of mass. The following relations are valid

$$r = c_p - c_v, \quad \kappa = \frac{c_p}{c_v} = 1.4, \quad (4)$$

where c_p and c_v are the specific heats at constant pressure and volume, respectively. The ratio of specific heat coefficients κ is so called Poisson's constant. From the thermodynamical analysis of continua is known, that the total energy per unit volume e of a system is the sum of its internal and its kinetic energy

$$e = \varrho \epsilon + \frac{1}{2} \varrho (u^2 + v^2). \quad (5)$$

The internal energy per unit of mass ϵ is a state variable of a system and for perfect gas is defined as $\epsilon = c_v T$, where T is thermodynamic temperature. The constitutive relation for static pressure p can be obtained, using the equations (3) – (5), in the form

$$p = (\kappa - 1) \left[e - \frac{1}{2} \varrho (u^2 + v^2) \right]. \quad (6)$$

2.2.1 Boundary conditions

The conservative system of the Euler equations (1) – (2) is, for example [5] or [2], quasi-linear and hyperbolic for each vector of conservative variables w . The number of the boundary conditions which have to be prescribed on the boundary of the computational domain $\Omega \subset \mathbb{R}^2$ is known from the theory of the hyperbolic equations. In our case of the two-dimensional sealing gap, when we assume the flow with subsonic inlet and subsonic outlet, we prescribe in the inlet section $\partial\Omega_I$ of the domain three physical boundary conditions:

- the inlet stagnation pressure $p_0 = 2 \cdot 10^5 \text{ Pa}$,
- the inlet stagnation temperature $T_0 = 293.15 \text{ K}$,
- the inlet angle α , which has to be computed from the geometry of the gap.

In the outlet section $\partial\Omega_O$ we prescribe one physical boundary condition:

- the outlet static pressure $p_2 = 10^5 Pa$.

On the solid impermeable walls of the domain $\partial\Omega_W$ the boundary condition $v^T \mathbf{n} = 0$ has to be satisfied, where \mathbf{n} is the outward unit normal vector to the boundary $\partial\Omega_W$.

2.3 Numerical solution of the system of the Euler equations

For the discretization of the conservative system of the Euler equations (1) – (2) the cell-centred finite volume method on a structured quadrilateral grid, Fig. 3, was used.

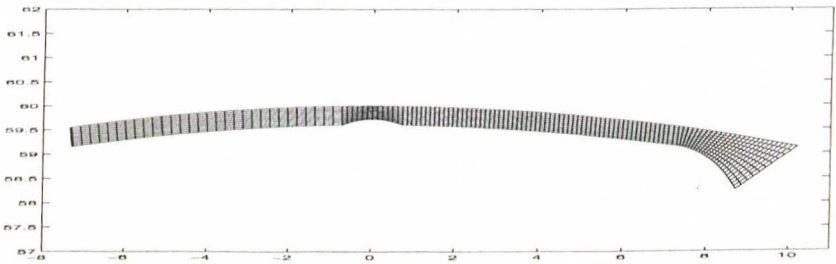


Fig. 3: Geometry of the sealing gap with a structured quadrilateral grid (128 × 10 cells)
 Bild 3: Geometrie des Gehäusespaltes mit einem viereckigen Gitter (128 × 10 Zellen)

In the finite volume method, nowadays very popular discretization technique for the Euler equations, the computational domain $\Omega \subset \mathbb{R}^2$ is subdivided into a finite number of small, non-overlapping, quadrilateral control volumes Ω_{ij} with the boundary $\partial\Omega_{ij}$, Fig. 4, that cover the whole computational domain Ω . Let us consider a partition $0 < t_0 < t_1 < t_2 < \dots < T$ of the time interval $(0, T)$ and set $\Delta t = t_{n+1} - t_n$.

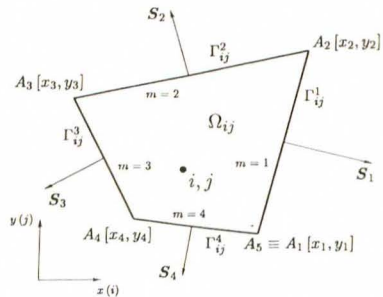


Fig. 4: Control volume Ω_{ij}
 Bild 4: Kontrollvolumen Ω_{ij}

On the control volume Ω_{ij} shown in Fig. 4, the exact solution $w(\mathbf{y}, t_n)$ at time t_n is approximated by a piecewise constant function w_{ij}^n , which should be considered as an approximation of the mean value of the exact solution $w(\mathbf{y}, t_n)$ over the cell Ω_{ij}

$$w_{ij}^n \approx \frac{1}{|\Omega_{ij}|} \int_{\Omega_{ij}} w(\mathbf{y}, t_n) d\mathbf{y}, \tag{7}$$

where $|\Omega_{ij}|$ denotes the face area of the cell Ω_{ij} . The value of the approximate solution w_{ij}^n

is associated to the centre (i, j) of the cell Ω_{ij} . The finite volume discretization of the Euler equations is based on the integration of the conservative system (1) over the set $\Omega_{ij} \times (t_n, t_{n+1})$. Using the Gauss-Ostrogradski's theorem we obtain

$$\int_{\Omega_{ij}} (w(\mathbf{y}, t_{n+1}) - w(\mathbf{y}, t_n)) d\mathbf{y} + \Delta t \oint_{\partial\Omega_{ij}} \mathcal{H}(w(\mathbf{y}, t_n)) \cdot \mathbf{n}_{ij} dS = 0, \quad (8)$$

where $\mathbf{n}_{ij} = (x_{n_{ij}}, y_{n_{ij}})^T$ denotes the outward unit normal vector to the boundary $\partial\Omega_{ij}$ of the cell Ω_{ij} and $\mathcal{H}(w(\mathbf{y}, t_n)) \cdot \mathbf{n}_{ij} = \mathbf{f}(w(\mathbf{y}, t_n)) x_{n_{ij}} + \mathbf{g}(w(\mathbf{y}, t_n)) y_{n_{ij}}$. The equation (8) can be approximated on the control volume Ω_{ij} , Fig. 4, by a finite volume scheme

$$\mathbf{w}_{ij}^{n+1} = \mathbf{w}_{ij}^n - \frac{\Delta t}{|\Omega_{ij}|} \sum_{m=1}^4 \mathcal{H}_m^n(w) \cdot \mathbf{S}_m, \quad (9)$$

where $\mathcal{H}_m^n(w) = (\mathbf{f}_m^n(w), \mathbf{g}_m^n(w))$ is the inviscid numerical flux through the edge Γ_{ij}^m of the cell Ω_{ij} at time t_n , Fig. 4, and $\mathbf{S}_m = (S_m^x, S_m^y)^T$ is the cell side normal vector to the edge Γ_{ij}^m . According to Fig. 4 we designate $\mathbf{S}_1 \equiv \mathbf{S}_{i+\frac{1}{2},j}$, $\mathbf{S}_2 \equiv \mathbf{S}_{ij+\frac{1}{2}}$, $\mathbf{S}_3 \equiv \mathbf{S}_{i-\frac{1}{2},j}$ and $\mathbf{S}_4 \equiv \mathbf{S}_{ij-\frac{1}{2}}$.

The aim of the numerical simulation is to obtain the steady state numerical solution of the conservative system of the Euler equations (1) – (2) in the space-time cylinder $\Omega_T = \Omega \times (0, T)$. We find the steady state solution with using the stationary boundary conditions mentioned in subsection 2.2.1 by means of a suitable time marching method for time $t \rightarrow \infty$. For the numerical solution of the conservative system of the Euler equations (1) – (2) we used the cell-centred finite volume formulation of the Causon's simplified TVD MacCormack scheme on an arbitrary structured quadrilateral grid, proposed in [1].

The classical explicit two-step MacCormack scheme approximates the finite volume scheme (8) in the following way

$$\begin{aligned} \mathbf{w}_{ij}^{n+\frac{1}{2}} &= \mathbf{w}_{ij}^n - \frac{\Delta t}{|\Omega_{ij}|} (\mathbf{f}_{i+1,j}^n S_{i+\frac{1}{2},j}^x + \mathbf{g}_{i+1,j}^n S_{i+\frac{1}{2},j}^y + \mathbf{f}_{ij+1}^n S_{ij+\frac{1}{2}}^x + \mathbf{g}_{ij+1}^n S_{ij+\frac{1}{2}}^y + \\ &+ \mathbf{f}_{ij}^n S_{i-\frac{1}{2},j}^x + \mathbf{g}_{ij}^n S_{i-\frac{1}{2},j}^y + \mathbf{f}_{ij}^n S_{ij-\frac{1}{2}}^x + \mathbf{g}_{ij}^n S_{ij-\frac{1}{2}}^y), \end{aligned} \quad (10)$$

$$\begin{aligned} \mathbf{w}_{ij}^{n+1} &= \frac{1}{2} \left\{ \mathbf{w}_{ij}^n + \mathbf{w}_{ij}^{n+\frac{1}{2}} - \frac{\Delta t}{|\Omega_{ij}|} \left[\mathbf{f}_{ij}^{n+\frac{1}{2}} S_{i+\frac{1}{2},j}^x + \mathbf{g}_{ij}^{n+\frac{1}{2}} S_{i+\frac{1}{2},j}^y + \mathbf{f}_{ij}^{n+\frac{1}{2}} S_{ij+\frac{1}{2}}^x + \right. \right. \\ &+ \left. \left. \mathbf{g}_{ij}^{n+\frac{1}{2}} S_{ij+\frac{1}{2}}^y + \mathbf{f}_{i-1,j}^{n+\frac{1}{2}} S_{i-\frac{1}{2},j}^x + \mathbf{g}_{i-1,j}^{n+\frac{1}{2}} S_{i-\frac{1}{2},j}^y + \mathbf{f}_{ij-1}^{n+\frac{1}{2}} S_{ij-\frac{1}{2}}^x + \mathbf{g}_{ij-1}^{n+\frac{1}{2}} S_{ij-\frac{1}{2}}^y \right] \right\}. \end{aligned} \quad (11)$$

It is well known, that the classical explicit numerical methods of the second-order accuracy, such as Lax-Wendroff or MacCormack schemes, generate high-frequency oscillations around sharp discontinuities. In order to stabilize the numerical solution in the shock region some artificial viscosity is needed. In our case, after the predictor (10) and corrector (11) steps of the finite volume formulation of the explicit MacCormack scheme, we add the TVD-type viscosity terms $d\mathbf{w}_{ij}^1$ and $d\mathbf{w}_{ij}^2$ to the numerical solution \mathbf{w}_{ij}^{n+1}

$${}^{(TVD)}\mathbf{w}_{ij}^{n+1} = \mathbf{w}_{ij}^{n+1} + d\mathbf{w}_{ij}^1 + d\mathbf{w}_{ij}^2, \quad (12)$$

where ${}^{(TVD)}\mathbf{w}_{ij}^{n+1}$ is the corrected numerical solution at time t_{n+1} . For the Causon's simplified TVD MacCormack scheme on an arbitrary structured quadrilateral grid the added dissipative

term dw_{ij}^1 can be written in the form, for example [5] or [1]

$$dw_{ij}^1 = [P_{ij}^+ + P_{i+1j}^-](w_{i+1j}^n - w_{ij}^n) - [P_{i-1j}^+ + P_{ij}^-](w_{ij}^n - w_{i-1j}^n), \quad (13)$$

$$P_{ij}^\pm \equiv P(r_{ij}^\pm) = \frac{1}{2}C(\nu_{ij})[1 - \Phi(r_{ij}^\pm)], \quad (14)$$

$$r_{ij}^\pm = \frac{(w_{i+1j}^n - w_{ij}^n, w_{ij}^n - w_{i-1j}^n)}{(w_{i+1j}^n - w_{ij}^n, w_{i+1j}^n - w_{ij}^n)}, \quad r_{ij}^- = \frac{(w_{i+1j}^n - w_{ij}^n, w_{ij}^n - w_{i-1j}^n)}{(w_{ij}^n - w_{i-1j}^n, w_{ij}^n - w_{i-1j}^n)}.$$

Note that in these relations (\cdot, \cdot) denotes the scalar product of two vectors. The functions $\Phi(r_{ij}^\pm)$ and $C(\nu_{ij})$ in the relation (14) are defined as

$$\Phi(r_{ij}^\pm) = \begin{cases} \min(2r_{ij}^\pm, 1) & \text{pro } r_{ij}^\pm > 0 \\ 0 & \text{pro } r_{ij}^\pm \leq 0 \end{cases}, \quad C(\nu_{ij}) = \begin{cases} \nu_{ij}(1 - \nu_{ij}) & \text{pro } \nu_{ij} \leq \frac{1}{2} \\ 0.25 & \text{pro } \nu_{ij} > \frac{1}{2} \end{cases}.$$

For ν_{ij} can be written the following formula

$$\nu_{ij} = \frac{\Delta t}{\Delta x_{ij}}(|u_{ij}| + a_{ij}), \quad (15)$$

where u_{ij} is the velocity in the direction i and a_{ij} is the local speed of sound. The time step Δt is given by the CFL condition (18) and Δx_{ij} and Δy_{ij} are the approximations of the lengths of the cell Ω_{ij} in the directions i and j computed as

$$\Delta x_{ij} = \frac{2|\Omega_{ij}|}{|S_{i+\frac{1}{2}j} - S_{i-\frac{1}{2}j}|}, \quad \Delta y_{ij} = \frac{2|\Omega_{ij}|}{|S_{ij+\frac{1}{2}} - S_{ij-\frac{1}{2}}|}. \quad (16)$$

For the added dissipative term dw_{ij}^2 we use similar formulae with the change of index j .

2.3.1 Convergence and stability of MacCormack scheme

The finite volume formulation of the Causon's simplified TVD MacCormack scheme (10) – (12) works as an iterative process, where an initial condition w_{ij}^0 has to be given. The convergence of the iterative process is measured by a residual which is computed as the discrete L_2 norm of the time derivative of density

$$Rez = \sqrt{\frac{\sum_{ij} |\Omega_{ij}| \left(\frac{e_{ij}^{n+1} - e_{ij}^n}{\Delta t} \right)^2}{\sum_{ij} |\Omega_{ij}|}}. \quad (17)$$

To describe the convergence history of the iterative process we plot a graph of the decimal logarithm of the values Rez in dependence on the number of iterations n . The iterative process will be stopped when Rez is less than a pre-selected value ε . It means that the steady state solution of the conservative system of the Euler equations (1) – (2) is reached when the condition $Rez < \varepsilon$ is fulfilled.

A necessary CFL condition for the stability of the explicit two-step MacCormack scheme is expressed by the restriction for the time step

$$\Delta t \leq \min_{(ij)} \left(\frac{\text{CFL}}{\frac{|u_{ij}| + a_{ij}}{\Delta x_{ij}} + \frac{|v_{ij}| + a_{ij}}{\Delta y_{ij}}} \right), \quad (18)$$

where $|u_{ij}| + a_{ij}$ and $|v_{ij}| + a_{ij}$ are the maximum absolute values of the eigenvalues of the Jacobian matrices $\mathbf{A} = \partial \mathbf{f}(\mathbf{w}) / \partial \mathbf{w}$ and $\mathbf{B} = \partial \mathbf{g}(\mathbf{w}) / \partial \mathbf{w}$ for the case of Euler's equations, $\text{CFL} \in (0, 1)$ and Δx_{ij} and Δy_{ij} are defined in (16).

3 Numerical results

The precise geometry of the sealing gap between the stator and the head of the female rotor tooth on a millimetre scale, filled with a structured quadrilateral grid can be seen in Fig. 3. For the numerical computation of the steady state fluid flow through the female rotor-housing gap the relatively fine structured grid with 1300×50 quadrilateral cells was used. Fig. 5 displays the Mach number profiles along lower (plotted with full line) and upper (plotted with dashed line) walls of the sealing gap computed with the above described cell-centred finite volume formulation of the explicit two-step Causon's simplified TVD MacCormack scheme after 381 200 iterations. It can be seen from Fig. 5 that the inlet Mach number is about $M_1 = 0.456$. The constant CFL in the necessary CFL condition (18) for the stability of the MacCormack scheme was chosen as $\text{CFL} = 0.5$. The Causon's simplified TVD MacCormack scheme converges poorly towards the stationary solution ($Rez \approx 10^{-2}$).

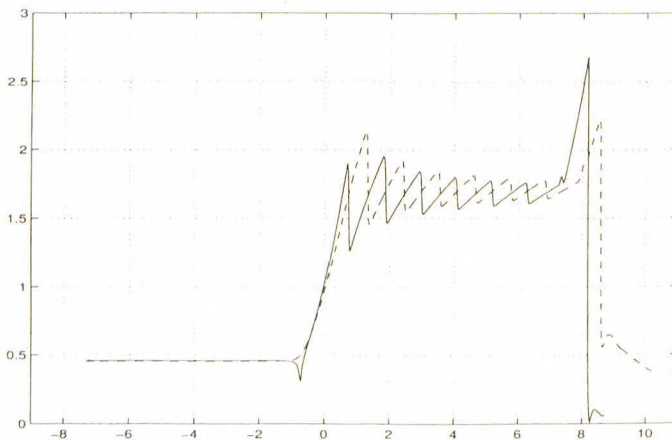


Fig. 5: Mach number profiles along lower and upper walls of the female rotor-housing gap
Bild 5: Mach-Zahlverlauf längs der unteren und oberen Wand des Gehäusespaltes

In Fig. 6, the isolines of the Mach number in the two-dimensional model of the female rotor-housing gap of the screw compressor are shown. The isolines are plotted with $\Delta M = 0.04$.

From Fig. 5 and Fig. 6, we can observe a subsonic region in the inlet part of the sealing gap up to the circular arc obstacle which represents a sealing strip. Above the circular bump the Mach number grows and the subsonic region changes to supersonic one, which occurs

in the part of the sealing gap behind the circular arc obstacle. First shock is obtained as the flow reaches the end of the circular bump. This shock is reflected from the upper and lower walls. The supersonic region is terminated by another shock obtained at the position where the female rotor-housing gap enlarges. The outflow is again subsonic.

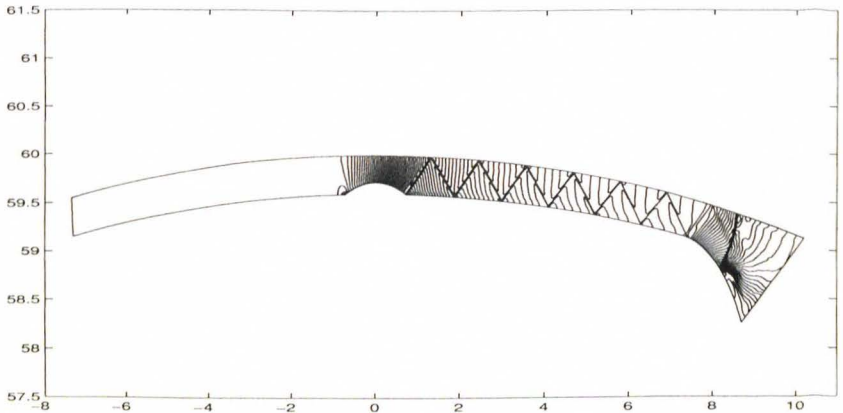


Fig. 6: Isolines (contours) of the Mach number in the female rotor-housing gap ($\Delta M = 0.04$)
Bild 6: Verteilung der Machzahl (Machzahlkonturen) im Gehäusespalt ($\Delta M = 0.04$)

In Fig. 7 and Fig. 8, the results of the numerical simulation of the compressible inviscid fluid flow in the sealing gap gained by using the software package Fluent 5.3 are presented. The numerical calculation was done for the same geometry of the female rotor-housing gap, Fig. 3, for the same boundary conditions described in subsection 2.2.1 (operating pressure = $0 Pa$, inlet gauge total pressure = $2 \cdot 10^5 Pa$, inlet total temperature = $293.15 K$, inlet direction specification method = normal to boundary, outlet gauge pressure = $10^5 Pa$) and on the same structured quadrilateral grid with 1300×50 cells. For the discretization a second order upwind scheme with Courant number = 0.5 was chosen.

Fig. 7 displays the Mach number profiles along lower and upper walls of the sealing gap after 75 000 iterations. In Fig. 8, the isolines of the Mach number in the two-dimensional model of the female rotor-housing gap of the screw compressor are shown. This numerical calculation converges very bad towards the stationary solution.

When we compare the numerical results of the steady state compressible inviscid fluid flow through the sealing gap obtained by means of the Causon's simplified TVD MacCormack scheme, Fig. 5, with the numerical results gained by using the software package Fluent 5.3, Fig. 7, we can see that these results are generally in good agreement (the same inlet Mach number $M_1 = 0.456$ and the similar supersonic region behind the circular bump). Only one difference can be observed. Namely, the different values of the maximal Mach number on the lower and upper walls at the position, where the female rotor-housing gap enlarges.

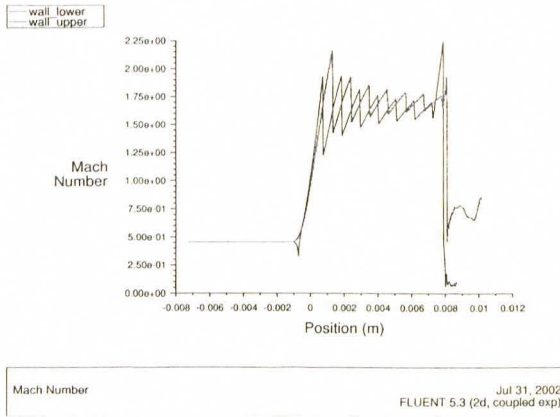


Fig. 7: Mach number profiles along lower and upper walls of the female rotor-housing gap
 Bild 7: Mach-Zahlverlauf längs der unteren und oberen Wand des Gehäusespaltes

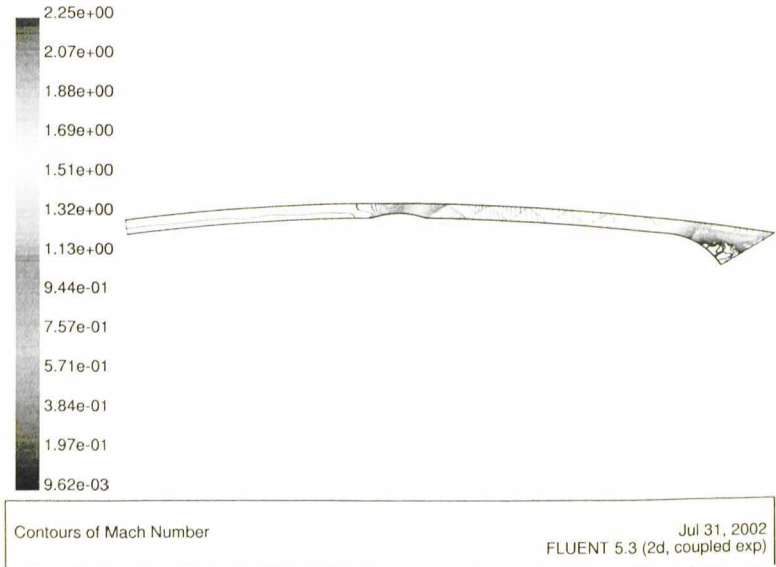


Fig. 8: Isolines of the Mach number in the female rotor-housing gap
 Bild 8: Verteilung der Machzahl im Nebenrotor-Gehäusespalt

In [6] we presented the results of the numerical simulation of the compressible inviscid fluid flow through the female rotor-housing gap obtained by means of the cell-centred finite volume formulation of the explicit two-step MacCormack scheme with Jameson's artificial dissipation on the structured quadrilateral grid with 700×30 cells. The numerical test was done for the different geometry of the sealing gap ($h = 0.6 h_v$, see Fig. 2) and the following boundary conditions were prescribed:

- the inlet stagnation pressure $p_0 = 5 \cdot 10^5 \text{ Pa}$,
- the inlet stagnation temperature $T_0 = 373.15 \text{ K}$,
- the inlet angle α , which has to be computed from the geometry of the gap,
- the outlet static pressure $p_2 = 10^5 \text{ Pa}$.

Fig. 9 displays the Mach number profiles along lower and upper walls of the female rotor-housing gap. It can be seen that the inlet Mach number is about $M_1 = 0.243$. The Courant number was chosen in this case as $\text{CFL} = 0.4$. The MacCormack scheme with Jameson's artificial dissipation converges also very bad towards the stationary solution.

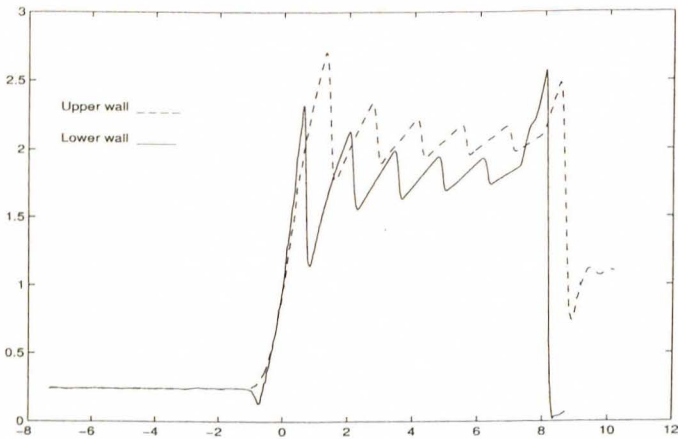


Fig. 9: Mach number profiles along lower and upper walls of the sealing gap ($h = 0.6 h_v$)
 Bild 9: Mach-Zahlverlauf längs der unteren und oberen Wand des Gehäusespaltes

In Fig. 10, the isolines of the Mach number distribution in the sealing gap are shown.

When we compare the numerical results illustrated in Fig. 5 and Fig. 6 with the numerical results from Fig. 9 and Fig. 10, we can see the influence of the sealing gap geometry and of boundary conditions on the steady state compressible inviscid fluid flow through the two-dimensional model of the female rotor-housing gap in the screw compressor.

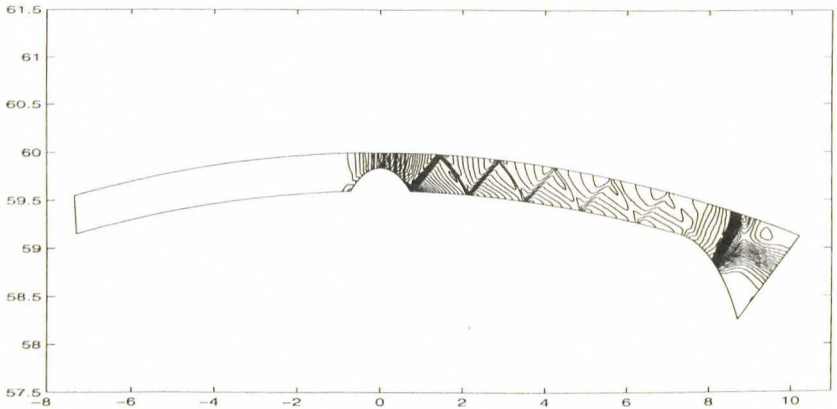


Fig. 10: Isolines (contours) of the Mach number in the female rotor-housing gap ($h = 0.6 h_v$)
 Bild 10: Verteilung der Machzahl (Machzahlkonturen) im Gehäusespalt ($h = 0.6 h_v$)

Abstractedly from our numerical computations, the experiment was performed at the Technical University of Dortmund, see [3]. In Fig. 11, a Schlieren picture of a gas flow in a two-dimensional model of the male rotor-housing gap of the screw compressor is presented. The Schlieren picture has been made for the pressure ratio $p_{ein}/p_{aus} = 2$ and the height of the sealing gap is $h = 0.4 \text{ mm}$.

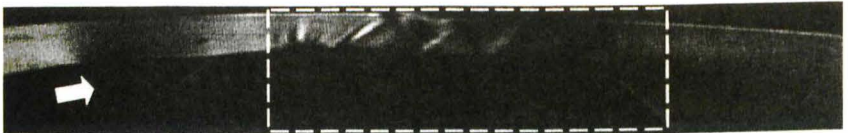


Fig. 11: Schlieren picture of the male rotor-housing gap, TU Dortmund
 Bild 11: Schlierenaufnahme des Hauptrotor-Gehäusespaltes, TU Dortmund

The flow visualisation gives a qualitative overview about the gas flow behaviour and it is useful in its characterisation. With regard to the large similarity of the female rotor-housing gap geometry used for our numerical simulation and of the male rotor-housing gap geometry used by the experiment and because of the same pressure ratio ($p_0/p_2 = 2$ and $p_{ein}/p_{aus} = 2$), we can confront our numerical results of the steady state compressible inviscid fluid flow, illustrated in Fig. 6, with the Schlieren picture from Fig. 11. It can be seen in both cases that the first shock wave, which occurs at the end of the sealing strip, is reflected from the upper and lower walls of the gap. So, we can deduce that our numerical results proportionally agree with the experiment.

4 Conclusions

In this paper the numerical simulation of the steady state compressible inviscid fluid flow through the two-dimensional model of the female rotor-housing gap in the screw compressor is presented. The obtained numerical results give us the first idea about the character of the gas flow through the sealing gap with the fixed lower wall which simulates a simplified situation when the female rotor does not move. It has been shown that the character of the gas flow through the gap highly depends on the precise geometry of the real sealing gap of the screw compressor and on the choice of the boundary conditions, which have to be prescribed on the boundary of the computational domain. All numerical methods which were used for the numerical simulation in this paper cover very bad towards the stationary solution.

It is necessary to mention that the problem of the gas flow through this narrow channel has to be solved by using the compressible viscous flow model. That is the reason that one can expect a fluid flow separation behind the circular bump. The aim of our further research in this area is to analyse the compressible viscous fluid flow through the female rotor-housing gap of the screw compressor. For the precise solution of this problem it would be very desirable the numerical simulation and an experiment for the same conditions to perform.

References

- [1] Causon, D.M.: *High Resolution Finite Volume Schemes and Computational Aerodynamics*. In Nonlinear Hyperbolic Equations - Theory, Computation Methods and Applications, volume 24 of Notes on Numerical Fluid Mechanics, pp. 63–74, Vieweg, Braunschweig, March 1989.
- [2] Hirsch, Ch.: *Numerical Computation of Internal and External Flows*, Vol. 1, 2. John Wiley & Sons, Chichester 1990.
- [3] Kauder, K., Arajo-Rudolph, L., Sachs, R.: *Experimentelle und numerische Untersuchung von Gasströmungen in einem ebenen Hauptrotor-Gehäusespaltmodell einer Schraubenmaschine*. Schraubenmaschinen - Heft Nr. 8/2000, ISSN 0945-1870, Universität Dortmund 2000.
- [4] Švígler, J., Vimmr, J.: *Einführungsstudie zur mathematischen Modellierung der Strömungen in Schraubenkompressoren*. Schraubenmaschinen - Heft Nr. 8/2000, ISSN 0945-1870, Universität Dortmund 2000.
- [5] Vimmr, J.: *Mathematical Modelling of Compressible Fluid Flow in Internal Aerodynamics*. Ph.D. Thesis, Faculty of Applied Sciences, University of West Bohemia, Pilsen 2002. (in Czech)
- [6] Vimmr, J.: *Mathematical Modelling of Compressible Inviscid Fluid Flow through a Sealing Gap in the Screw Compressor*. Mathematics and Computers in Simulation – MATCOM 2103, Elsevier Science B.V. on behalf of IMACS, 2002. (article in press)